



**Suppression of Metallic Conductivity of  
Single-Walled Carbon Nanotubes by Cycloaddition  
Reactions**

Mandakini Kanungo, *et al.*  
*Science* **323**, 234 (2009);  
DOI: 10.1126/science.1166087

**The following resources related to this article are available online at  
[www.sciencemag.org](http://www.sciencemag.org) (this information is current as of January 23, 2009 ):**

**Updated information and services**, including high-resolution figures, can be found in the online version of this article at:

<http://www.sciencemag.org/cgi/content/full/323/5911/234>

**Supporting Online Material** can be found at:

<http://www.sciencemag.org/cgi/content/full/323/5911/234/DC1>

This article **cites 34 articles**, 4 of which can be accessed for free:

<http://www.sciencemag.org/cgi/content/full/323/5911/234#otherarticles>

This article appears in the following **subject collections**:

Chemistry

<http://www.sciencemag.org/cgi/collection/chemistry>

Information about obtaining **reprints** of this article or about obtaining **permission to reproduce this article** in whole or in part can be found at:

<http://www.sciencemag.org/about/permissions.dtl>

grained polymer glass (18). Our results confirm that stress-induced mobility allows polymer glasses to flow; a 1000-fold increase in mobility very nearly resulted in a 1000-fold increase in the flow rate. These results also strongly support the reliability of probe reorientation as an indicator of polymer mobility during deformation. Figure 3 only includes data from single-step creep experiments; data from recovery and multistep creep experiments do not fall on the same curve. This finding suggests that no mechanical variable universally exhibits a simple relation with molecular mobility.

Because we measured the strain and segmental mobility locally, we were able to perform simultaneous measurements in different parts of an inhomogeneously deformed sample. Mobility changes in three different positions of a sample that necked during deformation are shown in Fig. 4. Plots of sample width and local strain versus time are shown in Fig. 4, A and B, and illustrate necking that begins at position a and then propagates toward positions b and c. Changes in mobility at positions a, b, and c are shown in Fig. 4C. At each position, mobility accelerates as the local strain rate increases; data from all three positions are quantitatively consistent with the master curve in Fig. 3. In a necked sample, molecular mobility is fastest in the shoulder, rather than the neck, even though the true stress in the neck is greater than any other region in the sample.

Polymer glasses are nonequilibrium thermodynamic systems, and we briefly discuss how this influences the interpretation of our measurements. Physical aging describes the change in mechanical properties that occurs over time because of the very slow molecular rearrangements in a glass (11); molecular motions have been shown to slow during physical aging (29). Mechanical experiments on polymer glasses have sometimes been interpreted as a reversal of physical aging, or “rejuvenation” (1, 9–12). We attribute the changes in mobility in our experiment to the combination of deformation-induced mobility and physical aging/rejuvenation. It appears that deformation-induced mobility is the much greater effect in these experiments. For example, the green curve in Fig. 4C shows a small mobility decrease in the first 30,000 s, which we attribute to physical aging. This mobility decrease is similar in magnitude to the decrease caused by physical aging in the undeformed sample during the same time period.

Concepts from the jamming field might be useful for describing the behavior of polymer glasses under stress (8). According to this view, one can unjam glasses either by raising the temperature or applying stress (8, 18, 30). In our experiments, temperature and stress had a qualitatively different effect on molecular mobility. A 1000-fold increase in mobility by deformation at constant temperature changed the KWW  $\beta$  to about 0.8 (Fig. 1D). In the absence of deformation, a 1000-fold increase in mobility occurred

when the temperature was increased by 18 K, but at this temperature  $\beta$  was unchanged at 0.32. Thus, stress not only increased mobility but also, in contrast to temperature, sharpened the distribution of relaxation times. In the low-stress regime in Fig. 2, temperature and stress both increased mobility without narrowing the distribution of relaxation times.

Our results quantify mobility changes in an actively deformed polymer glass and establish a quantitative connection between molecular mobility and macroscopic deformation. We find that mobility is not a function of instantaneous stress alone but can also depend on strain and the deformation history. Plastic flow appears to modify spatially heterogeneous dynamics in the glass, which suggests that there is a complex interplay between microscopic motions and flow. We anticipate that quantitative measurements of molecular mobility during deformation, coupled with appropriate microscopic theory, will lead to substantially improved predictions of the nonlinear deformation behavior of polymer glasses.

#### References and Notes

- H. E. H. Meijer, L. E. Govaert, *Prog. Polym. Sci.* **30**, 915 (2005).
- H. Eyring, *J. Chem. Phys.* **4**, 283 (1936).
- R. E. Robertson, *J. Chem. Phys.* **44**, 3950 (1966).
- M. C. Boyce, D. M. Parks, A. S. Argon, *Mech. Mater.* **7**, 15 (1988).
- C. P. Buckley, D. C. Jones, *Polymer* **36**, 3301 (1995).
- J. M. Caruthers, D. B. Adolf, R. S. Chambers, P. Shrikhande, *Polymer* **45**, 4577 (2004).
- K. Chen, K. S. Schweizer, *Europhys. Lett.* **79**, 26006 (2007).
- A. J. Liu, S. R. Nagel, *Nature* **396**, 21 (1998).
- A. F. Yee, R. J. Bankert, K. L. Ngai, R. W. Rendell, *J. Polym. Sci. Part Polym. Phys.* **26**, 2463 (1988).
- J. J. Martinez-Vega, H. Trumel, J. L. Gacounolle, *Polymer* **43**, 4979 (2002).

- L. C. E. Struik, *Physical Aging in Amorphous Polymers and Other Materials* (Elsevier, New York, 1978).
- G. B. McKenna, *J. Phys. Condens. Matter* **15**, 5737 (2003).
- L. S. Loo, R. E. Cohen, K. K. Gleason, *Science* **288**, 116 (2000).
- H.-N. Lee, K. Paeng, S. F. Swallen, M. D. Ediger, *J. Chem. Phys.* **128**, 134902 (2008).
- F. M. Capaldi, M. C. Boyce, G. C. Rutledge, *Phys. Rev. Lett.* **89**, 175505 (2002).
- A. V. Lyulin, B. Vorselaars, M. A. Mazo, N. K. Balabaev, M. A. J. Michels, *Europhys. Lett.* **71**, 618 (2005).
- R. A. Riggelman, H.-N. Lee, M. D. Ediger, J. J. de Pablo, *Phys. Rev. Lett.* **99**, 215501 (2007).
- R. A. Riggelman, K. S. Schweizer, J. J. de Pablo, *Macromolecules* **41**, 4969 (2008).
- Materials and methods are available as supporting material on Science Online.
- M. D. Ediger, *Annu. Rev. Phys. Chem.* **51**, 99 (2000).
- R. Bergman, F. Alvarez, A. Alegria, J. Colmenero, *J. Non-Cryst. Solids* **235**, 580 (1998).
- H. G. H. van Melick, L. E. Govaert, H. E. H. Meijer, *Polymer* **44**, 2493 (2003).
- E. J. Kramer, *J. Polym. Sci. Part B Polym. Phys.* **43**, 3369 (2005).
- M. L. Falk, J. S. Langer, *Phys. Rev. E* **57**, 7192 (1998).
- P. Schall, D. A. Weitz, F. Spaepen, *Science* **318**, 1895 (2007).
- E. R. Weeks, J. C. Crocker, A. C. Levitt, A. Schofield, D. A. Weitz, *Science* **287**, 627 (2000).
- F. Casas, C. Alba-Simionesco, H. Montes, F. Lequeux, *Macromolecules* **41**, 860 (2008).
- K. Chen, K. S. Schweizer, *Macromolecules* **41**, 5908 (2008).
- C. T. Thureau, M. D. Ediger, *J. Chem. Phys.* **116**, 9089 (2002).
- T. K. Haxton, A. J. Liu, *Phys. Rev. Lett.* **99**, 195701 (2007).
- This work was supported by NSF through grant NIRT-0506840. We thank K. Schweizer, J. Caruthers, G. Medvedev, J. de Pablo, and R. Riggelman for helpful discussions.

#### Supporting Online Material

www.sciencemag.org/cgi/content/full/1165995/DC1

Materials and Methods

Figs. S1 to S3

References

16 September 2008; accepted 18 November 2008  
10.1126/science.1165995

## Suppression of Metallic Conductivity of Single-Walled Carbon Nanotubes by Cycloaddition Reactions

Mandakini Kanungo,<sup>1</sup> Helen Lu,<sup>2</sup> George G. Malliaras,<sup>1</sup> Graciela B. Blanchet<sup>2\*</sup>

The high carrier mobility of films of semiconducting single-walled carbon nanotubes (SWNTs) is attractive for electronics applications, but the presence of metallic SWNTs leads to high off-currents in transistor applications. The method presented here, cycloaddition of fluorinated olefins, represents an effective approach toward converting the “as grown” commercial SWNT mats into high-mobility semiconducting tubes with high yield and without further need for carbon nanotube separation. Thin-film transistors, fabricated from percolating arrays of functionalized carbon nanotubes, exhibit mobilities >100 square centimeters per volt-second and on-off ratios of 100,000. This method should allow for the use of semiconducting carbon nanotubes in commercial electronic devices and provide a low-cost route to the fabrication of electronic inks.

Single-walled carbon nanotubes (SWNTs) are potential candidates for application in electronic devices (1–4). The most severe drawback in this effort has been that the as-synthesized SWNTs are a mixture of semi-

conducting (SC) and metallic (M) tubes, hindering their application in thin-film transistors (TFTs), where high mobility and on/off ratios are essential. The nascent SWNTs also form as bundles that need to be further dispersed. Numer-

ous approaches have been taken for the separation of M and SC tubes. Post treatments (5, 6) lead to a high degree of separation, but the extremely low concentration of tubes in the dispersing solvent hinders the formation of percolating SC-SWNT arrays. Burning off metallic tubes after fabrication with high currents leads to high-mobility devices but is neither controllable nor scalable (7).

An alternative approach is to manipulate the electronic properties of SWNT through covalent chemical functionalization (8); that is, disrupt the  $\pi$  bonding system ( $sp^2$ ) by converting some sites into  $sp^3$  carbon atoms (9, 10). Using such an approach, one should, in principle, be able to lower the conductivity of the M nanotubes significantly and achieve low off-currents while maintaining a mobility sufficiently high for good device performance. We show here that both these parameters can be simultaneously controlled by the degree of functionalization. Several methods that allow either anchoring atoms or molecules (reactants) to the carbon nanotube framework or selectively aligning nanotubes of specific types or chirality onto treated surfaces (11, 12) have been explored. When functionalization of the nanotube walls is achieved through the presence of a strong oxidizer or highly reactive radical species, electronic properties are significantly degraded (13). Finding an effective, low-cost method to eliminate or convert M-SWNT is essential to reduce off-currents. Snow's early work on TFTs using random percolating arrays of SWNT (2, 14) showed carrier mobilities of  $150 \text{ cm}^2/\text{Vsec}$  but on/off ratios far too low for

device applications. In an attempt to increase the on/off ratio, Bo *et al.* (15) constructed near-percolating SWNT arrays connected by organic semiconducting links. Although this method largely increased the on/off ratio ( $10^5$ ), it greatly reduced the device's mobility.

Recent theoretical (9, 10, 16–21) and experimental (22–24) studies point to sizeable differences in the electronic properties of SWNTs modified by monovalent relative to divalent (cycloaddition) chemical functionalization. The early work on monovalent functionalization (25, 26), shows that fluorine functionalization leads to highly resistive material with fluorination-induced strains and fractures in the tube walls (27). In more recent work, a preferential etching of M-SWNT was achieved using a mild fluorine gas-phase reaction (28) and sidewall functionalization of carbon nanotubes with diazonium salts (29, 30). Reports on divalent functionalization have focused on optical studies (22–24).

In this work, we show that high mobility and high on/off ratios can concurrently be achieved in a random array of percolating high-pressure CO (HiPco) tubes functionalized through a controlled cycloaddition reaction with fluorinated polyolefins. The “as grown” commercial nanotube mats are functionalized into a network of tubes that can then be dispersed in an organic solvent. The resulting “denser” semiconducting inks (denser by a factor of about 30), when coated as a percolating array, lead to high-mobility devices without requiring further nanotube separation.

We performed two separate [2+2] cycloaddition reactions of SWNTs; the first with perfluoro-2(2-fluorosulfonylethoxy) propyl vinyl ether (PSEPVE) and the second with perfluoro (5-methyl-3,6-dioxanon-1-ene) (PMDE) (31). The corresponding functionalized SWNTs are

referred as FSWNT-PSEPVE and FSWNT-PMDE. The results from TFTs fabricated with percolating arrays of functionalized tubes, which were spin-coated onto substrates, show mobilities of  $10 \text{ cm}^2/\text{Vsec}$  for FSWNT-PSEPVE and  $110 \text{ cm}^2/\text{Vsec}$  for FSWNT-PMDE, both with on/off ratios of  $10^5$ .

The effect of a systematic [2+2] cycloaddition reaction on the mobility and off-current ( $I_{\text{off}}$ ) of a percolating array of FSWNT is illustrated for FSWNT-PSEPVE in Fig. 1. The dramatic reduction of the  $I_{\text{off}}$  with increasing reactant concentration ( $c$ , the ratio of the moles of reactant that successfully reacted to the moles of SWNT) is key to this work. Devices fabricated from a percolating array of pristine HiPco tubes have high mobilities but also high  $I_{\text{off}}$ , which indicates that conduction pathways are dominated by metallic tubes (30, 32). Increasing PSEPVE functionalization led to a dramatic decrease in  $I_{\text{off}}$ , caused by a reduction in the number of metallic percolating pathways. For  $c < 0.01$ , high mobility is preserved, but  $I_{\text{off}}$  was reduced by almost 5 orders of magnitude as compared with pristine SWNTs. For  $0.01 < c < 0.02$ ,  $I_{\text{off}}$  decreased further, but the carrier mobility decreased as well. At higher reactant concentrations, the mobility dropped precipitously, which suggests that the electronic properties of the M and SC-SWNTs have changed considerably. The dependence of the on- and off-currents on channel length is shown in the inset to Fig. 1. The low  $I_{\text{off}}$  maintained at very small channel lengths further confirms the disappearance of conducting pathways between source and drain at a 0.018 degree of fluorination. Gate sweeps for FSWNT-PSEPVE and FSWNT-PMDE under optimum functionalization conditions at reactant/CNT concentration are shown in Fig. 2A for  $c = 0.012$  and Fig. 2B for  $c = 0.019$ . The field-effect mobilities deduced

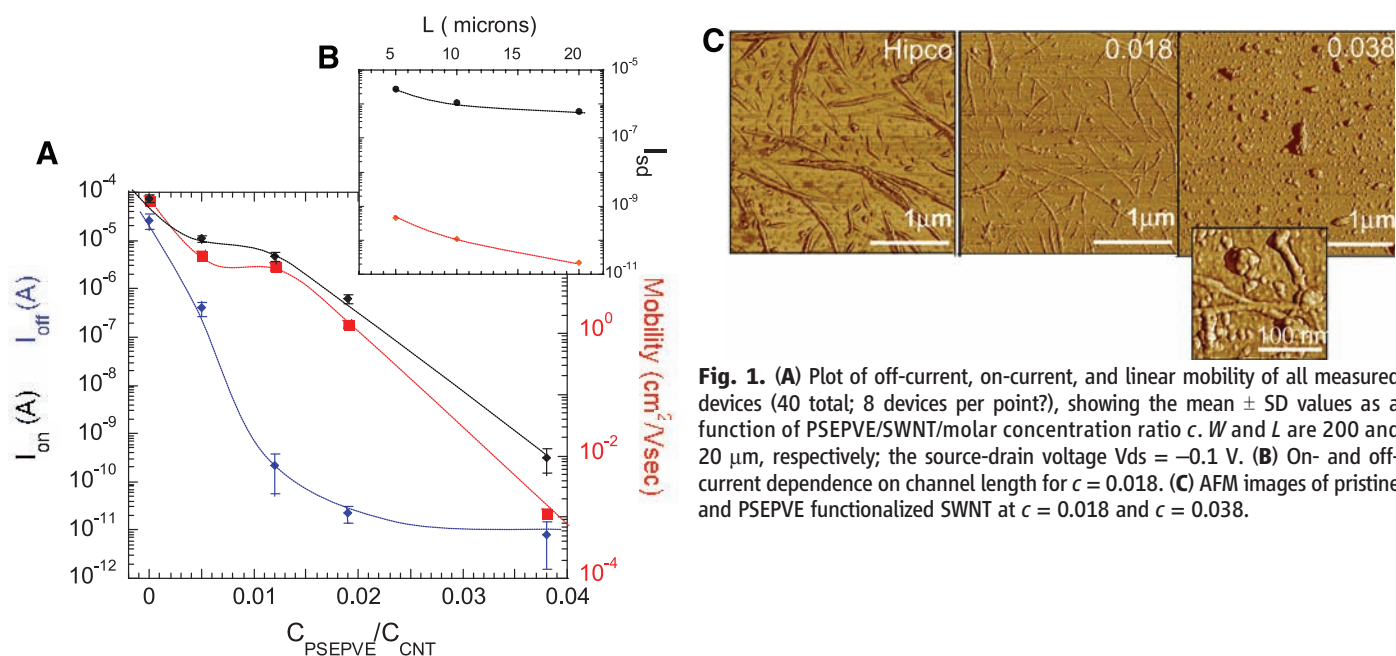


**Fig. 1.** (A) Plot of off-current, on-current, and linear mobility of all measured devices (40 total; 8 devices per point?), showing the mean  $\pm$  SD values as a function of PSEPVE/SWNT/molar concentration ratio  $c$ .  $W$  and  $L$  are 200 and 20  $\mu\text{m}$ , respectively; the source-drain voltage  $V_{\text{ds}} = -0.1 \text{ V}$ . (B) On- and off-current dependence on channel length for  $c = 0.018$ . (C) AFM images of pristine and PSEPVE functionalized SWNT at  $c = 0.018$  and  $c = 0.038$ .

<sup>1</sup>Cornell University, Department of Material Sciences, Ithaca, NY 14850, USA. <sup>2</sup>DuPont, Material Science and Engineering, Wilmington, DE 19880, USA.

\*To whom correspondence should be addressed. E-mail: graciela.b.blanchet@usa.dupont.com

from the linear regime are  $10 \text{ cm}^2/\text{Vsec}$  and  $110 \text{ cm}^2/\text{Vsec}$  with on/off ratios in excess of  $10^5$ .

To further understand the relative metallic content of the various fluorination levels, we studied the effect of the SWNT density on the electrical properties of the FSWNT arrays at the various functionalization levels (31). The network density, maintained above percolation, was varied from 8 to  $40 \text{ SWNT}/\mu^2$ . The effect of FSWNT density ( $\rho$ ) on electrical properties for  $c = 0.012$  is striking. At  $\rho = 35 \text{ tubes}/\mu^2$ ,  $I_{\text{off}}$  values comparable to those of bare HiPco reflect the formation of a percolating network of M tubes. At lower densities ( $\rho = 8.5$  and  $17.7 \text{ tubes}/\mu^2$ ),  $I_{\text{off}}$  drops by more than 4 orders of magnitude to  $10^{-10} \text{ A}$ , which reflects a sub-percolating concentration of M tubes. At slightly higher fluorination ( $c = 0.018$ ), the remaining M tubes appear to be fully removed. Low off-currents ( $10^{-10} \text{ A}$ ) can be maintained for both high-density arrays and low-channel-length transistors.

Atomic force microscopy (AFM) images of the pristine and functionalized arrays (Fig. 1B) show pristine HiPco (left) as well as lower and higher degrees of functionalization,  $c = 0.18$  (center) and  $c = 0.038$  (right). The HiPco ropes have largely exfoliated by  $c = 0.018$ , whereas at  $c = 0.038$  the tubes coalesce into nearly spherical particles, which consist of smaller particles  $\sim 20 \text{ nm}$  in diameter, as seen in the magnified inset.

To elucidate the origin of this SWNT transformation, we performed several analyses. Optical spectra (ultraviolet-visible-near-infrared, Fig. 3A) on mats treated with four different concentrations,  $c$ , display the transitions between the Van Hove singularities in the density of states that are characteristics of one-dimensional (1D) systems (33, 34). The broad features at 0.9 to 1.6 eV, associated with the  $E_{11}^S$  and  $E_{22}^S$  semiconducting transitions, remain practically unchanged for  $c < 0.02$ , where high mobility is also retained. In contrast, both  $E_{11}^S$  and  $E_{22}^S$  transitions disappear at higher levels of functionalization, indicating a deleterious effect of further functionalization on the SC tubes.

The Raman spectra in Fig. 3B show the disorder D and tangential G bands (12, 13, 35) in the  $1200$  to  $1700 \text{ cm}^{-1}$  region upon excitation at  $514 \text{ nm}$  for pristine and FSWNT-PSEPVE at  $c = 0.012$  and  $c = 0.019$ . The G band of semiconducting tubes consists of two peaks at  $1568 \text{ cm}^{-1}$  (radial) and at  $1591 \text{ cm}^{-1}$  (longitudinal). The G band spectrum of the metallic tubes also shows two bands at  $1589 \text{ cm}^{-1}$  (radial) and at  $1544 \text{ cm}^{-1}$  (longitudinal), the latter broadened into a Breit-Wigner Fano line shape caused by a strong coupling in the density of states. The spectra of Fig. 2B show that only the metallic band at  $1544 \text{ cm}^{-1}$  band is affected by functionalization, essentially disappearing for  $c \sim 0.02$ . Thus, the disappearance of the metallic band, concurrently with the decrease in  $I_{\text{off}}$  shown in Fig. 1, sug-

gests that cycloaddition in the low reactant regime primarily affects the M tubes. The intensity of the disorder D ( $\sim 1325 \text{ cm}^{-1}$ ) band also remains essentially unchanged in the low  $c$  regime.

In the present functionalization scheme, the presence of fluorine in the reactants helps in carrying out a divalent, 2-2 cycloaddition functionalization of the side wall. Having studied two reactants, PSEPVE and PMDE, gives us a means to understand whether the electrical changes are solely controlled by cycloaddition reaction or whether the side chain has an effect as well. The two side chains are nearly identical except that the PSEPVE side chain,  $\text{OCF}_2\text{CF}(\text{CF}_3)\text{OCF}_2\text{CF}_2\text{SO}_2\text{F}$ , has a sulfonic group whereas the PMDE side chain,  $\text{OCF}_2\text{CF}(\text{CF}_3)\text{OCF}_2\text{CF}_2\text{CF}_3$ , does not. The mobility of FSWNT-PMDE is  $\sim 10$  times as high as that of FSWNT-PSEPVE, which suggests that  $\text{SO}_2\text{F}$  leads to acid formation and doping.

A 60 to 70 Å square between cyclobutyl rings along the side walls is independent of the reactant concentration in the low-concentration regime (31). These data suggest that initially, the reactant anchors onto the walls of the ropes overcoming the Van der Waals interaction between tubes, inducing de-rope. We suggest that as the ropes exfoliate into smaller-diameter ropes, new sites become available and functionalization progresses, leading to further exfoliation until the status of single tubes is reached, with properties initially beneficial for electron transport. On the other hand, the high-resolution AFM for  $c = 0.038$  suggests that for high concentrations, single functionalized tubes have transitioned from an extended into a coiled conformation in a manner analogous to a rod-to-coil phase transition observed in many polymer systems. Indeed, the smaller spherical entities of  $\sim 20 \text{ nm}$  in diameter are similar in volume to that of a single tube of  $10 \text{ Å}$  diameter and  $0.6 \mu\text{m}$  in length.

From the electrical and optical data, we deduce that cycloaddition proceeds differently on M and SC SWNTs. In the low reactant regime ( $< 0.02$ )—of interest for devices—the optical and electrical data suggest that the M-SWNTs have been reduced, whereas the SC-SWNTs remain largely unaffected. This preferential modification of M tubes is probably caused by their much larger electron density near the Fermi level (22). Thus, cycloaddition of PSEPVE, in the low-concentration regime, either renders M-SWNTs inert or converts them into SC-SWNTs. The latter hypothesis is supported by the theoretical investigations of the effect of cycloaddition on the conductance of a metal carbon nanotube (10, 16, 18, 19) and by the work of Kamaras *et al.* (22).

We have developed a simple, high-yield method for the divalent functionalization of as-grown HiPco mats into preferentially semiconducting tubes with properties that are suitable for device applications. This work represents the first time that “bulk” quantities of commercial HiPco mats have been functionalized, dispersed into a high solid-content ink, and used to fab-

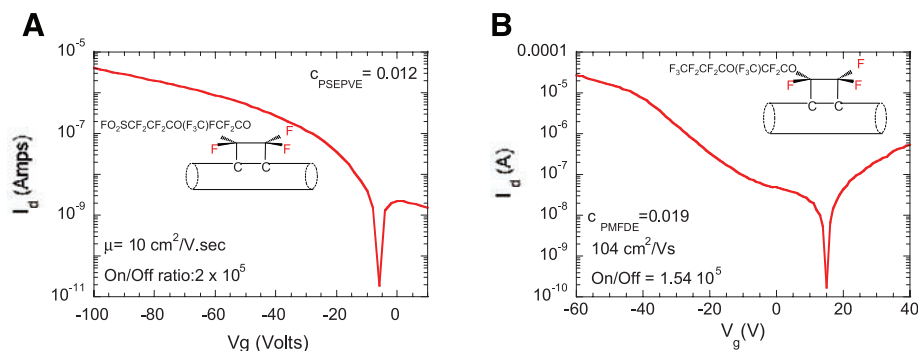


**Fig. 2.** Plot of source-drain current versus gate voltage for (A) FSWNT-PSEPVE and (B) FSWNT-PMFDE TFTs at  $c = 0.018$  and  $V_{\text{ds}} = -0.1 \text{ V}$  and  $-0.01 \text{ V}$ , respectively.

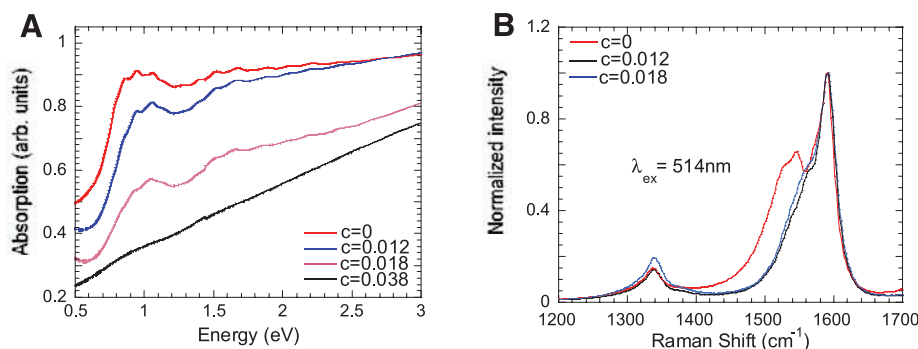


**Fig. 3.** (A) Optical spectra (of pristine HiPco tubes and the functionalized tubes). (B) Raman spectra of tangential and disorder mode region at 514-nm excitation wavelength. Spectra are normalized to the  $1591 \text{ cm}^{-1}$  band.

ricate percolating semiconducting arrays. We propose that, in the low concentration regime ( $c < 0.02$ ), cycloaddition provides an effective method to anchor molecules to the carbon nanotube framework and to either eliminate or transform metallic tubes. The data presented here suggest that  $c \sim 0.018$  fluorination level is sufficient to achieve the complete conversion of the metallic tubes without degrading the semiconducting tubes. The latter is a necessary step for the production of semiconducting inks suitable for printable electronics. While the cycloaddition reaction provides the anchoring sites, the long, highly fluorinated side chains are quite effective in exfoliating the ropes, thus enabling the effective conversion of M-SWNT even deep inside the ropes, as is necessary for achieving high-performance devices. We demonstrated the utility of the method by fabricating TFTs using percolating arrays of functionalized carbon nanotubes as the semiconducting layer with mobilities of  $100 \text{ cm}^2/\text{Vsec}$  and on/off ratios of  $10^5$ .

#### References and Notes

1. P. Avouris, Z. Chen, V. Perebeinos, *Nat. Nanotechnol.* **2**, 605 (2007).
2. E. S. Snow, P. M. Campbell, M. G. Ancona, *Appl. Phys. Lett.* **86**, 033105 (2005).
3. E. S. Snow *et al.*, *J. Vac. Sci. Technol. B* **22**, 1990 (2004).
4. E. Artukovic, M. Kaempgen, D. S. Hecht, S. Roth, G. Gruner, *Nano Lett.* **5**, 757 (2005).
5. H. Peng, N. T. Alvarez, C. Kittrell, R. H. Hauge, H. K. Schmidt, *J. Am. Chem. Soc.* **128**, 8396 (2006).
6. M. S. Arnold, A. A. Gree, J. F. Hulvat, S. I. Stupp, M. C. Hersam, *Nat. Mater.* **1**, 60 (2006).
7. P. G. Collins, M. S. Arnold, P. Avoris, *Science* **292**, 706 (2001).
8. M. S. Strano *et al.*, *Science* **301**, 1519 (2003).
9. J. Zhao, H. Park, J. Han, J. P. Lu, *J. Phys. Chem. B* **108**, 4227 (2004).
10. H. Park, J. Zhao, J. P. Lu, *Nano Lett.* **6**, 916 (2006).
11. R. Mclean, W. Huang, C. Khripin, A. Jogota, M. Zheng, *Nano Lett.* **6**, 55 (2006).
12. C. LeMieux *et al.*, *Science* **321**, 101 (2008).
13. Z. Chen, K. J. Ziegler, J. Shaver, R. H. Hauge, R. E. Smalley, *J. Phys. Chem. B* **110**, 11624 (2006).
14. E. S. Snow, J. P. Novak, P. M. Campbell, D. Park, *Appl. Phys. Lett.* **82**, 2145 (2003).
15. X.-Z. Bo *et al.*, *Appl. Phys. Lett.* **87**, 203510 (2005).
16. J. Zhao, Z. Chen, Z. Zhou, H. Park, P. R. Schyler, J. P. Lu, *Chem. Phys. Chem.* **6**, 598 (2005).
17. M. V. Veloso, A. G. Souza Filho, J. Mendes Filho, S. B. Fagan, R. Mota, *Chem. Phys. Lett.* **430**, 71 (2006).
18. Y.-S. Lee, N. Marzari, *J. Phys. Chem. C* **112**, 4480 (2008).
19. Y.-S. Lee, N. Marzari, *Phys. Rev. Lett.* **97**, 116801 (2006).
20. K. A. Park, Y. S. Choi, C. Kim, Y. H. Lee, *Phys. Rev. B* **68**, 045429 (2003).
21. J. Lu *et al.*, *J. Phys. Chem. B* **110**, 5655 (2006).
22. K. Kamaras, M. E. Itkis, H. Hu, B. Zhao, R. C. Haddon, *Science* **301**, 1501 (2003).
23. H. Hu *et al.*, *J. Am. Chem. Soc.* **125**, 14893 (2003).
24. C. Menard-Moyon, N. Izard, E. Doris, C. Mioskowski, *J. Am. Chem. Soc.* **128**, 6552 (2006).
25. K. S. Kim *et al.*, *Adv. Mater.* **14**, 1818 (2002).
26. K. H. An *et al.*, *Appl. Phys. Lett.* **80**, 4235 (2002).
27. H. F. Bettinger, K. N. Kudin, G. E. Scuseria, *J. Am. Chem. Soc.* **123**, 12849 (2001).
28. C.-M. Yang *et al.*, *Phys. Rev. B* **73**, 075419 (2006).
29. N. Nair, W.-J. Kim, M. L. Usrey, M. S. Strano, *J. Am. Chem. Soc.* **129**, 3946 (2007).
30. C. Wang *et al.*, *J. Am. Chem. Soc.* **127**, 11460 (2005).
31. Materials and methods are available as supporting material on Science Online.
32. J. Vavro, J. M. Kikkawa, J. E. Fischer, *Phys. Rev. B Condens. Matter* **71**, 155410 (2005).
33. A. Hagen, G. Moos, V. Talalaev, T. Hertel, *Appl. Phys. A* **78**, 1137 (2004).
34. J. Chen *et al.*, *Science* **282**, 95 (1998).
35. M. S. Dresselhaus, G. Dresselhaus, R. Saito, *Phys. Rep.* **409**, 47 (2005).
36. Supported by Air Force grant FA9550-071-0411. We thank H. L. Stormer and G. D. Jaycox for careful reading of the manuscript; R. Wheland for many interesting discussions; and D. Walls, J. Wyre, and N. G. Tassi for Raman, x-ray photoelectron spectroscopy, and high-resolution AFM inset at  $c = 0.038$ , respectively.

#### Supporting Online Material

[www.sciencemag.org/cgi/content/full/323/5911/234/DC1](http://www.sciencemag.org/cgi/content/full/323/5911/234/DC1)

Materials and Methods

Figs. S1 to S5

18 September 2008; accepted 19 November 2008

10.1126/science.1166087

# Self-Organization of a Mesoscale Bristle into Ordered, Hierarchical Helical Assemblies

Boaz Pokroy, Sung H. Kang, L. Mahadevan, Joanna Aizenberg\*

Mesoscale hierarchical helical structures with diverse functions are abundant in nature. Here we show how spontaneous helicity can be induced in a synthetic polymeric nanobristle assembling in an evaporating liquid. We use a simple theoretical model to characterize the geometry, stiffness, and surface properties of the pillars that favor the adhesive self-organization of bundles with pillars wound around each other. The process can be controlled to yield highly ordered helical clusters with a unique structural hierarchy that arises from the sequential assembly of self-similar coiled building blocks over multiple length scales. We demonstrate their function in the context of self-assembly into previously unseen structures with uniform, periodic patterns and controlled handedness and as an efficient particle-trapping and adhesive system.

**N**on-centrosymmetric chiral, coiled, and spiral configurations are ubiquitous in nature, spanning from amino acids to mollusk shells to galaxies (1). On a mesoscopic scale, such structures are abundant in biology, and these are usually composed of helical fibers that are often further assembled into higher-order hierarchical materials. Natural examples include DNA helices, amyloid fibers (2), cellulose fibrils in wood (3), hierarchy in bone (4, 5), and chirally

spinning nodal cilia (6), to name a few, with implications on a variety of functions from information transfer to mechanical integrity and control of the body symmetry in morphogenesis. Man-made coiled and spiral materials and designs on a macroscopic scale are widely used in our everyday life—from ropes and bolts to helicopter rotors. On the molecular scale, chirality plays a critical role in asymmetric chemical synthesis and catalysis (7), liquid crystals (8), supramolecular chemistry (9, 10), and organic and inorganic crystal engineering (11). Artificial coiled structures at the mesoscale are rare, and these usually have simple geometries of one-dimensional helical fibers and ribbons (1, 8–10, 12). At any length scale, twist and handedness in superstructures gener-

ally originate from either the assembly of non-centrosymmetric building blocks or the application of a chiral field or template (1–5, 8–13). Here we report on the induction of capillarity-driven self-organization of a nanobristle into helical clusters and demonstrate the fabrication of non-trivial, hierarchically assembled, coiled mesostructures over large areas, in which neither the assembling elements nor the environment are chiral, guided by and consistent with simple theoretical considerations.

Our approach is presented in Fig. 1A. We consider a periodic array of nanopillars, each of which is anchored at one end on a substrate and free at the other. A locally stable configuration of the bristles is just a uniform array of non-interacting straight pillars (first-order structures). However, this is not necessarily a globally stable state: When the array is immersed in a liquid that is then evaporated, capillary forces associated with the liquid/vapor menisci between the free ends of the geometrically soft bristles may cause them to deform laterally and adhere to each other. The effect of elastocapillary coalescence (14) has been described for a well-known phenomenon of clumping in wet hair (15) or paintbrush immersed in paint (16). Similar clustering behavior is observed in nature in the examples of the tarsi of beetles (17) and spiders (18). The morphology and dynamics of the ensuing structures are a result of the competition between intrapillar elasticity and inter-pillar adhesion (14–16). Individual pillars that are long enough can bend easily to accommodate the capillary forces associated with the menisci between adjacent pillars.

School of Engineering and Applied Sciences, Wyss Institute for Biologically Inspired Engineering, Harvard University, Cambridge, MA 02138, USA.

\*To whom correspondence should be addressed. E-mail: [jaiz@seas.harvard.edu](mailto:jaiz@seas.harvard.edu)